coatings

MDPI

Article

Residual Stresses in Soft Magnetic FeTiB and FeZrN Films Obtained by Magnetron Deposition

Valentin A. Tedzhetov [1], Elena N. Sheftel [1], Eugene V. Harin [1] and Philipp V. Kiryukhantsev-Korneev [2,*]

[1] Baikov Institute of Metallurgy and Materials Science RAS, Leninsky Prospekt 49, 119334 Moscow, Russia; vtedzhetov@imet.ac.ru (V.A.T.); sheftel@imet.ac.ru (E.N.S.); harin-eugene@ya.ru (E.V.H.)

[2] Department of Powder Metallurgy & Functional Coatings, National University of Science & Technology "MISIS", Leninsky prospect 4, 119049 Moscow, Russia

* Correspondence: kiruhancev-korneev@yandex.ru; Tel.: +7-495-638-4659

Abstract: The coercive field of soft magnetic ferromagnets is a structure-sensitive property and, in particular, is substantially affected by residual stresses. In the present study, the phase and structural states and residual stresses of the FeTiB and FeZrN films of various compositions, which were prepared by magnetron deposition on glass substrates and subsequent 1-h annealing at temperatures of 200–600 °C, were investigated by X-ray diffraction. The formation of a nanocrystalline structure is observed. It comprises different phases having different lattice parameters and unit-cell volumes and is characterized by high level of microstrains of grains as well; the microstrains predetermine the formation of high compressive stresses in the deposited films. As the annealing temperature increases, the compressive stresses decrease, and, at certain temperatures, gradually the films transform into thermal tensile stresses, which are induced by the difference in the thermal expansion coefficients of the film and substrate. Thus, the heat treatment is the efficient way to improve the soft magnetic properties of the studied class of film materials produced by magnetron deposition.

Keywords: soft magnetic films; magnetron deposition; nanocrystalline materials; X-ray diffraction; residual stress; phase composition

Citation: Tedzhetov, V.A.; Sheftel, E.N.; Harin, E.V.; Kiryukhantsev-Korneev, P.V. Residual Stresses in Soft Magnetic FeTiB and FeZrN Films Obtained by Magnetron Deposition. *Coatings* **2021**, *11*, 34. https://doi.org/10.3390/coatings11010034

Received: 9 December 2020
Accepted: 28 December 2020
Published: 31 December 2020

1. Introduction

The development of new magnetic materials that meet the ever-growing requirements of modern magnetic electronics is the important problem of materials science. In particular, information technology devices require soft magnetic film materials providing the combination of a maximum possible saturation induction (B_s > 2 T) and a low coercive field (H_c < 1 Oe).

Films of Fe-Ti-B and Fe-Zr-N system alloys with two-phases nanocrystalline structure (TiB_2 boride or ZrN nitride particles located in the main soft magnetic αFe phase), which are produced by magnetron deposition followed by annealing (300–500 °C), are able to ensure the combination of high saturation induction (B_s ~ 2 T) and low coercive field (H_c < 1 Oe) [1,2].

Such a class of film materials is prepared by magnetron sputtering. Energy parameters of the magnetron sputtering, unlike those of other preparation methods available for film materials [3], ensure the conditions for the preparation of films in amorphous and nanocrystalline states, which comprise high-temperature and thermodynamically stable phases, in particular, TiB_2 and ZrN.

The value of the coercive field is determined by the magnetic anisotropy energy, which includes contributions of the magnetocrystalline anisotropy (the anisotropy of crystal lattice of a material or its constituent phases) and magnetoelastic anisotropy (the magnetostriction, microstrains in the grain body of crystalline phases, and residual stresses).

Two main types of residual stresses can be induced in the films; these are the so-called intrinsic residual stresses formed in the course of magnetron deposition and thermal stresses, σ_T, formed during annealing of films. The intrinsic residual stresses are related to accumulated defects (crystal lattice distortions, stacking faults, impurity atoms, vacancies, etc.) and the evolution of the film structure during deposition [4]. The thermal stresses arise due to the difference in the thermal expansion coefficients of film and substrate materials [5].

The insight into quantitative relationships between residual stresses formed in ferromagnetic films and parameters of their phase and structural states allows the value of the coercive field of film material to be purposefully controlled. The present work is aimed at the study of quantitative relationships between residual stresses and parameters of the phase and structural states, which are realized in the FeTiB and FeZrN films prepared by magnetron deposition followed by annealing.

There are different methods for the determination of residual stresses; these are the nanoindentation [6], determination of substrate curvature [7], FIB-DIC method (focused ion beam-digital image correlation) [8], and X-ray diffraction $\sin^2\psi$ method [8]. The following advantages of the X-ray diffraction can be considered, which determine its application in term of the present work: the method is non-destructive and allows the stresses to be determined at a depth less than 1 μm, and the value of stresses to be averaged over the diffracting volume.

2. Materials and Methods

The FeTiB films were prepared by a DC magnetron sputtering of a composite target, which consists of a Fe disk with uniformly arranged TiB_2 plated. The process is performed in an argon atmosphere at a pressure of P_{Ar} = 0.2–0.3 Pa, at the voltage U = 500–600 V and the current I = 1.5–1.7 A. To prepare the FeZrN films, the reactive magnetron sputtering is used. In this case, the Fe target with metallic Zr plates arranged on its surface along the erosion zone was sputtered in a gas mixture (Ar + N_2) atmosphere at P_{Ar+N2} = 0.13–0.15 Pa, U = 450 V, and I = 1.5 A. The films were deposited on glass substrates 1.5 mm thick.

The substrate temperature during deposition did not exceed 200 °C. The chemical composition of the deposited films was determined by energy-dispersive X-ray spectroscopy and glow-discharge optical emission spectroscopy (GDOES). The film thickness was measured by scanning electron microscopy (SEM). The detailed descriptions of the preparation conditions and results of the chemical analysis of the films are reported in References [1,9]. The films were annealed in a vacuum (at a residual pressure of less than 3×10^{-4} Pa) for 1 h at temperatures of 200, 300, 400, 500, and 600 °C.

The phase analysis and the structural studies were performed by X-ray diffraction (XRD) using a Rigaku Ultima IV diffractometer equipped with a graphite monochromator, in the Bragg–Brentano geometry, using CuKα radiation; the scanning was carried out in a 2θ angular range of 20–120° at a step of 0.2°. The use of radiation from a tube equipped with a copper anode was due to the low penetration of the radiation (~2 μm) into the Fe-based material, which results from the large coefficient of linear attenuation. The software package [10] was applied for processing the experimental data using a full-profile Rietveld method. The phase composition, volume fractions of crystalline phases (ν_i), their lattice parameters (a/c), and structure of the films (size corresponding to grain size D and the Gaussian rms microstrains ε of the crystal lattice at the grain scale) were determined using XRD patterns. The lattice parameters of phases were determined from the position of the centers of gravity of high-angle peaks using the Voigt approximation.

The magnitude and sign of the residual stresses were determined using the $\sin^2\psi$ method [11]. It is known that arising the residual stresses in a material results in uniform changing the interplanar spacings Δd_{hkl} and, therefore, to shifting X-ray diffraction reflections. The $\sin^2\psi$ method is based on the measuring of the change in the position of reflections when patterns are taken at different angles ψ made by the sample surface normal and lattice plane normal. The obtained dependence of the angular position of reflection on $\sin^2\psi$ is described by the expression:

$$\theta_\psi = \theta_{\psi=0} - \frac{1+\nu}{E} tg\theta_{\psi=0} \sigma \sin^2\psi \quad (1)$$

where θ_ψ, $\theta_{\psi=0}$ are the angular positions of diffraction reflections at different angles ψ; ν is the Poisson's ratio; and E is the Young's modulus. In this case, the change in position of the high-angle peak (211) of αFe was recorded while the angle ψ is changed in the sequence 0, 20.7, 30.0, 37.8, 45.0, 52.2, and 60.0°.

The measurement was performed by iso-inclination method [12]. The CrKα radiation characterized by the highest wavelength (2.2898 Å) was used because it provides a possibility to record the (211) peak at high angles 2θ~156° and, thereby, to reduce the error of determination of the stress value. The dependences of the change in the angular position 2θ of the (211) peak on $\sin^2\psi$ were approximated by a linear function (Figure 1). The residual stresses were calculated using the Young's modulus (E_f = 175 GPa) of the studied films and Poisson's ratio of pure αFe (ν_f = 0.29).

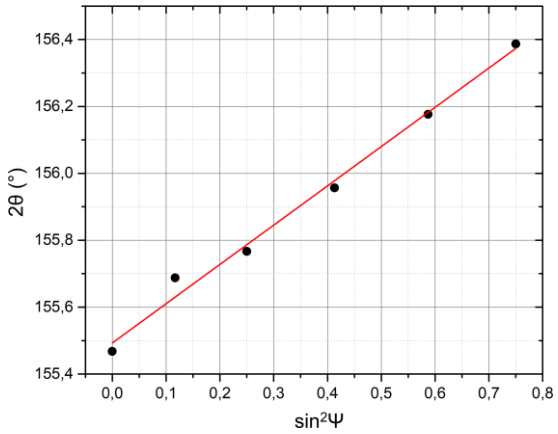

Figure 1. Linear approximation of the $2\theta_{(211)}$ dependence on $\sin^2\psi$ for the Fe film.

3. Results and Discussion

3.1. Chemical Composition of the Films

The distribution of chemical elements across the film thickness was determined by GDOES (Figure 2a); the averaged chemical compositions of each film under study are given in Table 1. The film thickness was measured using a SEM (Figure 2b). Thus, the films of the ternary FeTiB and FeZrN alloys and Fe (Table 1), the thickness of which is from 0.9 to 1.8 μm (Figure 2b), were prepared; the content of impurity oxygen in the films did not exceed 1.5–2 at.%.

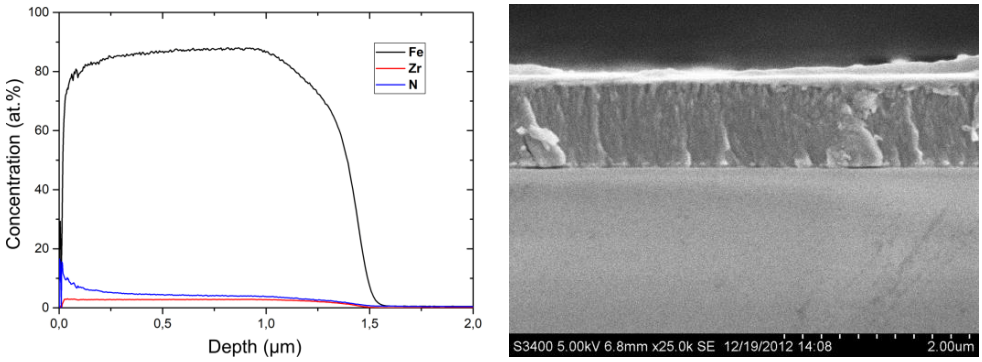

(**a**) (**b**)

Figure 2. (**a**) Distribution of elements (GDOES) and (**b**) micrograph (SEM) of the cross section of the $Fe_{92.2}Zr_{3.0}N_{4.8}$ film.

3.2. Phase Composition of the Deposited Films

The full-profile XRD patterns taken for all deposited films (Figure 3) exhibit two intense peaks observed at 2θ angles of ~44.5° and ~82°, which are close to the angular positions of (110) and (211) reflections of body-centered cubic (bcc) αFe and are shifted to the lower angles. The shift of the peaks means the formation of a phase with the bcc crystal structure, the lattice parameter (2.890 Å for the $Fe_{91.6}Ti_{3.0}B_{5.4}$ film and 2.904 Å for the $Fe_{92.2}Zr_{3.0}N_{4.8}$ film) of which exceeds the tabulated value for αFe (2.866 Å), Table 1. The higher intensity of the (110) peak of the phase, as compared to that of the (110) peak for the αFe standard indicates the formation of the <011> texture in these films. The diffraction patterns taken for the $Fe_{91.6}Ti_{3.0}B_{5.4}$ films exhibit an additional intense (200) peak of αFe observed at 2θ ~ 64.4°, which indicates a pronounced <001> axial texture of these films. This indicates the formation of bcc αFe-based solid solutions, compositions of which, αFe(Ti) and αFe(Zr,N), in the corresponding films were studied in detail in our previous works [1,9]. Using the diffraction patterns of the $Fe_{91.6}Ti_{3.0}B_{5.4}$ and $Fe_{88.7}Zr_{4.4}N_{6.9}$ films, containing the largest amounts of alloying elements (Ti and B or Zr and N), the peaks of additional phases (Fe_2B boride with a tetragonal body-centered lattice and Fe_4N nitride with a face-centered cubic lattice, respectively (Figure 3, Table 1)) were identified. The volume fraction of additional phases does not exceed 0.42.

The XRD patterns of all films contain a wide (integral linewidth of more than 7°) diffuse peak, the angular position of which approaches that of the most intense reflection of αFe (~44.5°, inset in Figure 3). This indicates the formation of a mixed amorphous-crystalline structure in the films.

Upon deposition, a nanocrystalline structure is formed in all films. For single-phase films, the grain size of the bcc phase depends on content of alloying element in the bcc phase; so the grain size of the phase in the FeTiB films (~24–34 nm) is higher than that in the FeZrN films (~13 nm) (Table 1). The effect of the content of alloying element in the αFe-based solid solution on its grain size is confirmed by the biggest grains of the αFe phase in Fe films (~46 nm) (Table 1).

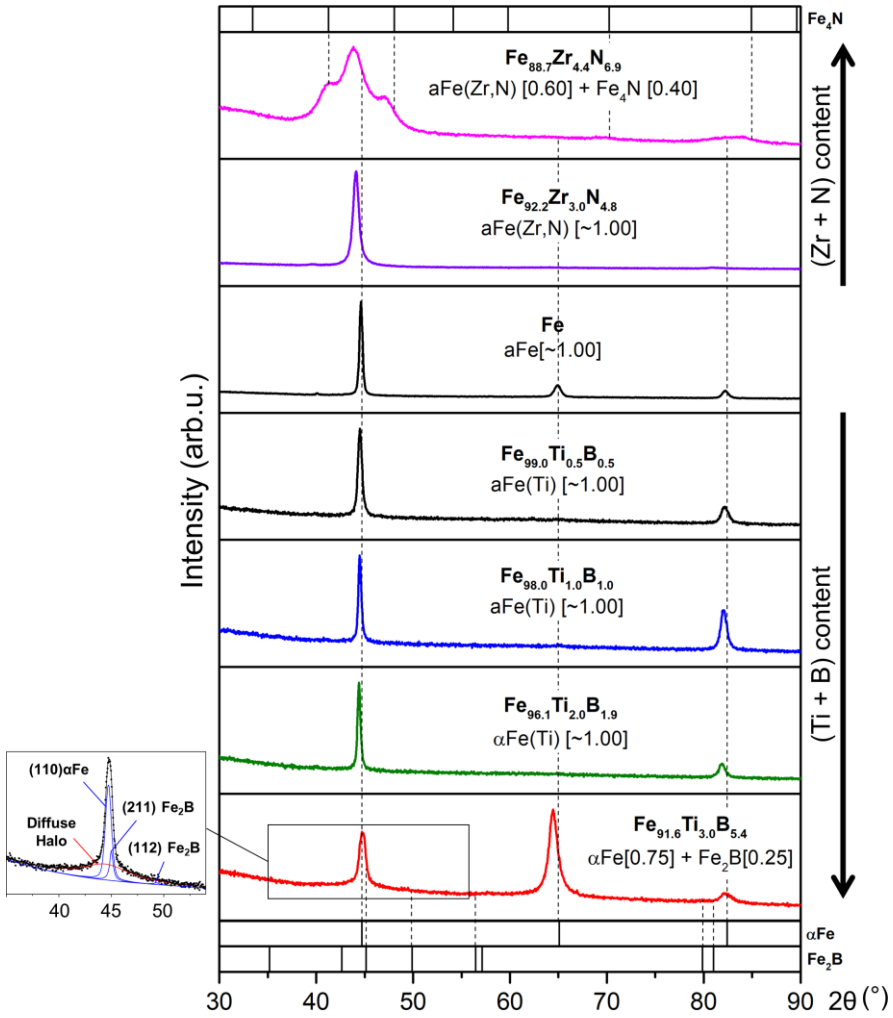

Figure 3. XRD patterns of the as-deposited films under study.

The grain size of the bcc phase in two-phase films is much smaller (8 nm and 2 nm in FeTiB and FeZrN films, respectively) as compared to those in the single-phase films (Table 1). It can be assumed that, upon deposition of two-phase films, the high-temperature phases Fe_2B and Fe_4N phases condense on the substrate before the bcc phase, and, thus, prevent the growth of the bcc phase grains.

It should be noted that the high microstrains are formed in the grains (~0.2–0.3% in the bcc phase grains and ~0.4–0.7% in grains of the boride and nitride phases, Table 1).

3.3. Phase Composition of the Annealed Films

The qualitative estimation of XRD patterns taken for the deposited and annealed films indicates that, after annealing, no significant changes in the reflections of the bcc phase and the boride–nitride phase are observed. This testifies the fact that the principal phase composition of the films was formed in the course of deposition process. The appearance of the third phase (αFe + Fe_3N + ZrO_2) in the $Fe_{88.7}Zr_{4.4}N_{6.9}$ films after annealing at 600 °C is associated with the occurrence of diffusion processes at the film–glass (SiO_2) interface. However, the quantitative estimations of the XRD patterns taken for all films indicate that, as annealing temperature increases, the lattice parameter of the bcc phase decreases; however, the lattice parameter retain higher than the tabulated lattice parameter of αFe, 2.866 Å, (Table 1). It means that, as annealing temperature increases, a slight depletion of the bcc solid solution in alloying elements occurs. The stability of the film structure formed

during deposition is evidenced by both a slight increase in the phase grain sizes and a slight decrease in the microstrain in the grains after annealing.

Table 1. Phase composition and structure of the studied films in as-deposited and annealed states.

Film	T_{ann}, °C	ν_i Phase	*a*/*c*, Å	*D*, nm	ε, %
Fe	As-dep.	~1.00 αFe	2.872	45.6	0.268
$Fe_{99.0}Ti_{0.5}B_{0.5}$	As-sput.	~1.00 αFe(Ti)	2.879	24.4	0.247
-	200	~1.00 αFe(Ti)	2.877	24.7	0.248
-	300	~1.00 αFe(Ti)	2.874	26.1	0.256
-	400	~1.00 αFe	2.866	31.2	0.264
-	500	~1.00 αFe	2.866	32.4	0.250
$Fe_{98.0}Ti_{1.0}B_{1.0}$	As-sput.	~1.00 αFe(Ti)	2.879	35.5	0.237
-	200	~1.00 αFe(Ti)	2.880	35.9	0.247
-	300	~1.00 αFe(Ti)	2.876	38.2	0.242
-	400	~1.00 αFe(Ti)	2.879	36.4	0.230
-	500	~1.00 αFe(Ti)	2.875	34.3	0.279
$Fe_{96.1}Ti_{2.0}B_{1.9}$	As-sput.	~1.00 αFe(Ti)	2.885	34.1	0.205
-	200	~1.00 αFe(Ti)	2.883	38.5	0.229
-	300	~1.00 αFe(Ti)	2.879	30.7	0.187
-	400	~1.00 αFe(Ti)	2.878	27.4	0.216
-	500	~1.00 αFe(Ti)	2.871	34.5	0.239
$Fe_{91.6}Ti_{3.0}B_{5.4}$	As-sput.	0.75 αFe	2.890	8.2	0.160
		0.25 Fe_2B	–	22.7	0.399
-	200	0.69 αFe	2.890	8.4	0.365
		0.31 Fe_2B	–	–	–
-	300	0.76 αFe	2.892	8.3	0.177
		0.24 Fe_2B	–	–	–
-	400	0.72 αFe	2.889	8.4	0.127
		0.28 Fe_2B	–	–	–
-	500	0.80 αFe	2.874	8.3	0.203
		0.20 Fe_2B	5.114/4.229	44.7	0.331
$Fe_{92.2}Zr_{3.0}N_{4.8}$	As-sput.	~1.00 αFe(Zr,N)	2.904	13.6	0.247
-	300	~1.00 αFe(Zr,N)	2.900	14.0	0.301
-	400	~1.00 αFe(Zr,N)	2.898	14.8	0.270
-	500	~1.00 αFe(Zr,N)	2.883	18.4	0.300
-	600	~1.00 αFe(Zr,N)	2.877	21.4	0.302
$Fe_{88.7}Zr_{4.4}N_{6.9}$	As-sput.	0.58 αFe(Zr,N)	2.887	2.0	0.066
		0.42 Fe_4N	3.818	5.5	0.745
-	400	0.61 αFe(Zr,N)	2.887	2.0	0.093
		0.39 Fe_4N	3.821	6.7	0.635
-	500	0.51 αFe(Zr,N)	2.872	2.9	0.131
		0.49 Fe_4N	3.793	8.2	0.482
-	600	0.28 αFe(Zr,N)	2.864	14.6	0.038
		0.57 Fe_3N	–	3.4	0.164
		0.15 ZrO_2	5.087	3.7	0.379

Note, that TiB and TiB_2 phases in the FeTiB films were not identified although the chemical compositions of these films are close to the stoichiometry Ti:B~1:1 and ~1:2, respectively. The predominance of kinetic factors in the course of the film deposition probably explains this fact. It is also possible that the sensitivity of the XRD method is insufficient to identify a small volume of fine-grained phase.

3.4. Residual Stresses in the Films

The significant compressive stresses (up to ~1.5 GPa) are formed in all deposited films (Figure 4). According to data of [13], residual stresses in the deposited films arise either owing to the difference in coefficients of thermal expansion of the film and substrate

(thermal stresses σ_T) or owing to the formation of crystallographic defects in a film material (so-called intrinsic stresses). According to data of [14], the dominant type of stresses is determined by the value of the ratio T_s/T_m, where T_s (K) is the substrate temperature and T_m (K) is the film material melting point. The thermal stresses, σ_T, prevail at $T_s/T_m > 0.3$; intrinsic stresses prevail at $T_s/T_m < 0.3$.

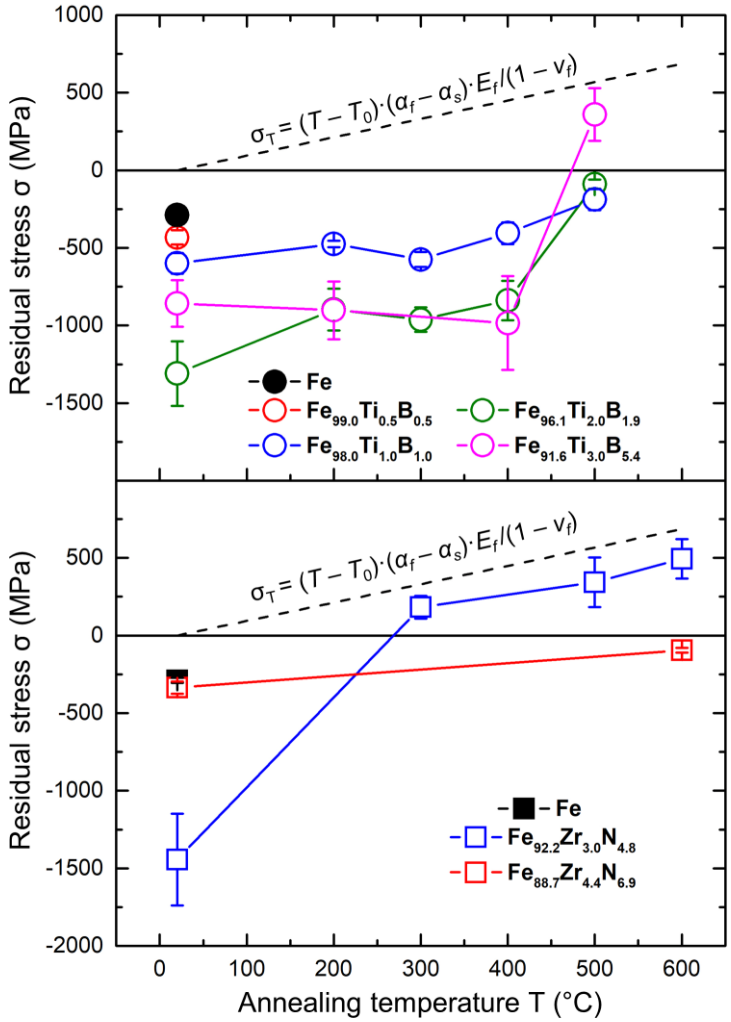

Figure 4. Dependences of the residual stresses in the studied films on the annealing temperature. The dashed lines show dependence (3).

Since the melting temperature of the studied films is close to that of iron (1812 K) (the studied films contain at least 88 at.% Fe), and the substrate temperature is 473 K, the ratio T_s/T_m for the deposited films equals ~0.26, i.e., it is less than 0.3; therefore, the intrinsic stresses should prevail in the deposited films. This assumption agrees with experimental data obtained for the deposited films, namely, with the formation of αFe-based supersaturated solid solutions, formation of phases with different crystal lattice parameters (2.866 Å for αFe, 5.100/4.240 Å for Fe_2B, and 3.790 Å for Fe_4N), and unit-cell volumes (23.55 $Å^3$ for αFe, 110.8 $Å^3$ for Fe_2B, and 54.44 $Å^3$ for Fe_4N) and with high level of microstrain in the grains as well (Table 1).

During annealing, as the temperature increases, the compressive stress values decrease and approach zero (Figure 4). The sign of stresses changes to the opposite at 500 °C for the $Fe_{91.6}Ti_{3.0}B_{5.4}$ films and at 300 °C for the $Fe_{92.2}Zr_{3.0}N_{4.8}$ films, and the further increase in the temperature results in the formation of tensile stresses of at least 500 MPa. The transition from compressive to tensile stresses after annealing in the temperature range of 300–500 °C was previously observed by us for similar films [15].

It is natural to assume that thermal stresses, σ_T, should prevail in the annealed films. The thermal stresses appear due to the difference in the thermal expansion coefficients of iron α_f and glass α_s (substrate material). The comparison of these values [16,17] gives the inequality:

$$\alpha_f\,(11.8 \times 10^{-6}\ \mathrm{K}^{-1}) > \alpha_s\,(7 \times 10^{-6}\ \mathrm{K}^{-1}) \quad (2)$$

therefore, according to [5], tensile thermal stresses, σ_T, should form in the studied films. The magnitude of σ_T is described by the dependence

$$\sigma_T = (T - T_0)\cdot(\alpha_f - \alpha_s)\cdot E_f/(1 - \nu_f) \quad (3)$$

where T is the annealing temperature and T_0 is the room temperature. The dashed lines in Figure 4 graphically represent the dependence (3).

In accordance with (3), the thermal stresses σ_T can reach 686 MPa in the film cooled from a temperature of 600 °C. This is in good agreement with the experimentally obtained values of stresses in the studied films annealed at 500 and 600 °C. Thus, the linear dependence (3), plotted as a dashed line in Figure 4, indicates that, as the annealing temperature increases, the contribution of σ_T to the resulting stresses formed in the films becomes predominant.

It should be noted that the possibility to reduce or eliminate residual stresses in the films and thereby to reduce the magnitude of the coercive field of the film via the heat treatment is the efficient way to improve the soft magnetic properties of the film material.

4. Conclusions

1. The phase and structural states and the residual stresses of the FeTiB and FeZrN films of various compositions, which were prepared by magnetron deposition on glass substrates and subsequent 1-h annealing at temperatures of 200–600 °C, were studied by X-ray diffraction.
2. Depending on the content of alloying elements, Ti and B or Zr and N, in the Fe-based films, a single-phase (bcc αFe(Ti) and αFe(Zr,N) solid solutions) or two-phase (bcc solid solution + Fe_2B boride or Fe_4N nitride) nanocrystalline structure are formed during deposition. The grain size varies (2–46 nm) in accordance with the chemical and phase compositions of the films. All films exhibit the high level of microstrains in grains (~0.2–0.3% for the bcc phase; ~0.4–0.7% for Fe_2B and Fe_4N). The structure formed upon deposition is stable during heating.
3. The significant compressive stresses (up to ~1.5 GPa) are formed in all deposited films, which are associated with the formation of αFe-based supersaturated solid solutions in the films, phases with markedly different lattice parameters and unit-cell volumes, and with the high microstrains in the nanograins of the phases as well. As the annealing temperature increases, the values of the compressive stresses decrease, gradually approaching zero, and after that, compressive stresses change into tensile ones, which are related to the different thermal expansion coefficients of iron and glass.
4. The heat treatment is the efficient way in order to improve the soft magnetic properties of the studied class of film materials produced by magnetron deposition.

Author Contributions: Conceptualization, E.N.S.; formal analysis, V.A.T. and E.V.H.; investigation, V.A.T.; resources, P.V.K.-K.; writing—original draft preparation, V.A.T., E.N.S. and E.V.H.; writing—review and editing, V.A.T. and E.V.H.; visualization, P.V.K.-K.; project administration, E.N.S. All authors have read and agreed to the published version of the manuscript.

Funding: This research was funded by Russian Foundation for Basic Research, grant number 18-03-00502a.

Institutional Review Board Statement: Not applicable.

Informed Consent Statement: Not applicable.

Data Availability Statement: The data presented in this study are available in this article.

Conflicts of Interest: The authors declare no conflict of interest.

References

1. Sheftel, E.N.; Harin, E.V.; Tedzhetov, V.A.; Kiryukhantsev-Korneev, P.V.; Levashov, E.A.; Perov, N.S.; Titova, A.O. Magnetic structure and magnetic properties of nanocrystalline and amorphous Fe-Zr-N films. *Phys. B Condens. Matter* **2016**, *494*, 13–19. [CrossRef]
2. Sheftel, E.N.; Tedzhetov, V.A.; Harin, E.V.; Kiryukhantsev-Korneev, F.V.; Usmanova, G.S. High-induction nanocrystalline soft magnetic $Fe_XTi_YB_Z$ films prepared by magnetron sputtering. *Phys. Status Solidi C* **2016**, *13*, 965–971. [CrossRef]
3. Bunshah, R.F. *Handbook of Deposition Technologies for Films and Coatings*, 2nd ed.; Noyes Publications: Park Ridge, NJ, USA, 1994.
4. Detor, A.J.; Hodge, A.M.; Chason, E.; Wang, Y.; Xu, H.; Conyers, M.; Nikroo, A.; Hamza, A. Stress and microstructure evolution in thick sputtered films. *Acta Mater.* **2009**, *57*, 2055–2065. [CrossRef]
5. Wang, H.J.; Deng, H.A.; Chiang, S.Y.; Su, Y.F.; Chiang, K.N. Development of a process modeling for residual stress assessment of multilayer thin film structure. *Thin Solid Film.* **2015**, *584*, 146–153. [CrossRef]
6. Zhou, W.; Zhou, H.; Zhang, R.; Pei, Y.; Fang, D. Measuring residual stress and its influence on properties of porous ZrO_2/(ZrO_2+Ni) ceramics. *Mater. Sci. Eng. A* **2015**, *622*, 82–90. [CrossRef]
7. Injeti, S.S.; Annabattula, R.K. Extending Stoney's equation to thin, elastically anisotropic substrates and bilayer films. *Thin Solid Film.* **2016**, *598*, 252–259. [CrossRef]
8. Bemporad, E.; Brisotto, M.; Depero, L.E.; Gelfi, M.; Korsunsky, A.M.; Lunt, A.J.G.; Sebastiani, M. A critical comparison between XRD and FIB residual stress measurement techniques in thin films. *Thin Solid Film.* **2014**, *572*, 224–231. [CrossRef]
9. Sheftel', E.N.; Tedzhetov, V.A.; Kiryukhantsev-Korneev, F.V.; Harin, E.V.; Usmanova, G.S.; Zhigalina, O.M. Investigation of the Processes of the Formation of a Nonequilibrium Phase-Structural State in FeTiB Films Obtained by Magnetron Sputtering. *Russ. J. Non-Ferr. Met.* **2020**, *61*, 753–761. (in press). [CrossRef]
10. Shelekhov, E.V.; Sviridova, T.A. Programs for X-ray analysis of polycrystals. *Metal Sci. Heat Treat.* **2000**, *42*, 309–313. [CrossRef]
11. Noyan, I.C.; Cohen, J.B. *Residual Stress: Measurement by Diffraction and Interpretation*; Springer-Verlag: New York, NY, USA 1987.
12. Hanabusa, T.; Suzuki, K.; Akita, K. *Standard Method for X-ray Study*; The Society of Materials Science: Kyoto, Japan, 2005.
13. Carneiro, J.O.; Teixeira, V.; Azevedo, S. Residual Stresses in Thin Films Evaluated by Different Experimental Techniques. In *Encyclopedia of Thermal Stresses*, 1st ed.; Hetnarski, R.B., Ed.; Springer: Amsterdam, The Netherlands, 2014; Volume 1, pp. 4222–4231. [CrossRef]
14. Zeman, H.; Musil, J.; Vlček, J.; Mayrhofer, P.H.; Mitterer, C. Thermal annealing of sputtered Al-Si-Cu-N films. *Vacuum* **2003**, *72*, 21–28. [CrossRef]
15. Sheftel, E.N.; Ivanov, A.N.; Usmanova, G.S. X-ray diffraction study of the evolution of phase and structural state and macroscopic stress during annealing of soft magnetic $Fe_{95-x}Zr_5N_x$ films prepared by ion-plasma deposition. *Crystallogr. Rep.* **2014**, *59*, 266–275. [CrossRef]
16. Touloukian, Y.S.; Kirby, R.K.; Taylor, R.E.; Desai, P.D. Thermal Expansion–Metallic Elements and Alloys. In *Thermophysical Properties of Matter–the TPRC Data Series*; IFI/Plenum Press: New York, NY, USA, 1975; Volume 12.
17. Touloukian, Y.S.; Kirby, R.K.; Taylor, R.E.; Lee, T.R. Thermal Expansion–Nonmetallic Solids. In *Thermophysical Properties of Matter—The TPRC Data Series*; IFI/Plenum Press: New York, NY, USA, 1977; Volume 13.